International Journal of Mass Spectrometry 435 (2019) 7–17

Contents lists available at ScienceDirect

International Journal of Mass Spectrometry

journal homepage: www.elsevier.com/locate/ijms

Full Length Article

Short-lived intermediates (encounter complexes) in cisplatin ligand exchange elucidated by infrared ion spectroscopy

Davide Corinti[a], Cecilia Coletti[b], Nazzareno Re[b], Roberto Paciotti[b], Philippe Maître[c], Barbara Chiavarino[a], Maria Elisa Crestoni[a], Simonetta Fornarini[a,*]

[a] Dipartimento di Chimica e Tecnologie del Farmaco, Università di Roma "La Sapienza", I-00185 Roma, Italy
[b] Dipartimento di Farmacia, Università G. D'Annunzio, I-66100 Chieti, Italy
[c] Laboratoire de Chimie Physique, Université Paris-Sud, UMR 8000 CNRS, 91405 Orsay, France

ARTICLE INFO

Article history:
Received 18 July 2018
Received in revised form
27 September 2018
Accepted 2 October 2018
Available online 4 October 2018

Dedicated to Helmut Schwarz on the occasion of his 75th birthday honoring his contribution in gas-phase ion chemistry and in science

Keywords:
Platinum(II) complexes
Non-covalent complexes
IRMPD spectroscopy
Photodissociation
Reaction mechanism
DFT calculations

ABSTRACT

Cisplatin (*cis*-diamminedichloroplatinum(II), *cis*-$[PtCl_2(NH_3)_2]$), widely used drug in cancer treatment, has been allowed to react with simple molecular targets (L) mimicking biological functional groups. The selected molecules (L = acetamide, dimethylacetamide, urea and thiourea) react by ligand exchange leading to *cis*-$[PtCl(NH_3)_2(L)]^+$ complexes that have been assayed by ESI-MS, IRMPD spectroscopy and computations in order to characterize their structure and platination site. Formal five-coordinate complexes are also delivered by ESI, $[(PtCl(NH_3)_2(H_2O)(L)]^+$, notably absent only when L is thiourea. IRMPD spectroscopy combined with computational analysis has revealed non-covalent adducts of the reactant aqua complex with an external ligand L corresponding to $\{cis\text{-}[PtCl(NH_3)_2(H_2O)]^+ \cdot L\}$, reminiscent of the Eigen-Wilkins encounter complex invoked in the ligand displacement path in solution. The complex, successfully isolated in the gas phase, undergoes ligand exchange yielding *cis*-$[PtCl(NH_3)_2(L)]^+ + H_2O$ when activated by multiple IR photons, testifying at the same time both structure and reactivity.

1. Introduction

The chemistry of platinum is relevant in a large variety of contexts. One of them is catalysis, where both elemental platinum and platinum complexes perform paramount roles. Understanding the elementary steps and significant intermediates involved in catalytic activity is a complex task and makes a highly ambitious goal. Remarkable insight has been revealed by mechanistic studies in the well defined gaseous environment as reported by Helmut Schwarz and his group [1–9]. Kinetic and thermodynamic data regarding exemplary platinum cations have also been provided [10–13].

In the present contribution another side of platinum activity is approached, namely the bioinorganic chemistry of cisplatin, a widely used antitumor drug [14]. Cisplatin (cis-diamminedichloroplatinum(II), cis-$[PtCl_2(NH_3)_2]$) exerts anticancer activity by platination of DNA, following a sequence of steps involving transport into the cell and aquation (replacement of a chloro with an aqua ligand) [15–17]. On its way to final attack to DNA, cisplatin is exposed to reaction with a number of biomolecular targets that may act as cisplatin carriers but are also held responsible for drug resistance and adverse effects [18–20]. An understanding of the molecular mechanisms at play may aid in the development of new compounds in the family of platinum antitumor drugs, combining greater efficacy with less drawbacks.

Electrospray ionization (ESI) has proven a viable means to release the primary ionic intermediates formed from cisplatin in aqueous solution as naked gaseous species [21,22]. The ensuing gas phase ion chemistry has allowed us to unveil aspects of cisplatin interaction with biomolecules, such as amino acids, or with simplified models possessing relevant functional groups. The earliest aqua complexes from hydrolysis of both cis- and transplatin, *cis*- and *trans*-$[PtCl(NH_3)_2(H_2O)]^+$, obtained as free ions in the gas phase, have been characterized by infrared multiphoton dissociation (IRMPD) spectroscopy allowing clear isomeric discrimination

* Corresponding author.
E-mail address: simonetta.fornarini@uniroma1.it (S. Fornarini).

https://doi.org/10.1016/j.ijms.2018.10.012

[23]. The reactivity of *cis*- and *trans*-$[PtCl(NH_3)_2(H_2O)]^+$ has been compared with the one of the hydroxo counterparts, *cis*- and *trans*-$[[Pt(OH)(NH_3)_2(H_2O)]^+$ in a direct assay that has only been accessed in the gas phase study allowing isolation and sampling strictly of the species of interest [24]. IRMPD spectroscopy has offered appropriate means to unveil the interaction of cisplatin derived ions with building blocks of DNA (nucleobases and nucleotides) [25–27]. The hitherto not yet characterized primary complexes from cisplatin attack at the aminoacids that are preferred platination targets in peptides and proteins, namely histidine (His) and methionine (Met), also examined via their vibrational spectroscopic features, have displayed competing sites in proportions that have been estimated by IRMPD kinetics data [28,29].

In a direction towards simplification of the complex biological environment faced by cisplatin and derived species, simple molecules (L) holding key biochemical functional groups have been selected and allowed to react with cisplatin [30]. ESI has thus afforded not only substitution complexes where a chloro ligand has been replaced by L but also formally five-coordinate complexes of the general formula $[PtCl(NH_3)_2(H_2O)(L)]^+$. These species have been examined by a combined approach using both IRMPD spectroscopy and collision induced dissociation (CID) experiments, interpreted with the support of theoretical calculations. The emerging pattern displays a structure for $[PtCl(NH_3)_2(H_2O)(L)]^+$ ions whereby an external L molecule is non-covalently bound to the four-coordinate *cis*-$[PtCl(NH_3)_2(H_2O)]^+$ complex. The non-covalent cluster thus displays the nature of an Eigen-Wilkins encounter complex, lying on the reaction coordinate for the ligand substitution reaction (Eq. (1)).

$$\textit{cis}\text{-}[PtCl(NH_3)_2(H_2O)]^+ + L \rightarrow \{\textit{cis}\text{-}[PtCl(NH_3)_2(H_2O)]^+ \cdot L\} \rightarrow \textit{cis}\text{-}[PtCl(NH_3)_2(L)]^+ + H_2O \quad (1)$$

According to this recognized mechanistic model, ligand (L) exchange on a complex such as $[M(H_2O)_n]^{m+}$ occurs after rapid formation of an outer sphere encounter complex, $\{[M(H_2O)_n]^{m+} \cdot L\}$, bound by electrostatic interactions. The formation of this complex is diffusion controlled and the rate limiting event is typically the L/H_2O interchange between the first and the second coordination sphere within the encounter complex [31–35]. Evidence on the role of this complex in solution is mainly based on kinetics and thus the ESI formed ion provides an unprecedented opportunity to clarify its structure and mechanistic role. It appeared of interest to verify any general occurrence of these species and to inquire about (i) what properties of the ligand L may allow delivery of $[PtCl(NH_3)_2(H_2O)(L)]^+$ ions by ESI from aqueous solution and (ii) what is the structure and relative stability of potential isomers that may account for the ion at the observed *m/z* value. To this end $[PtCl(NH_3)_2(L)(H_2O)]^+$ ions have been investigated by CID and IRMPD spectroscopy and the experimental results analyzed in combination with the outcome of theoretical calculations.

2. Experimental and theoretical methods

2.1. Sample preparation

Stock solutions of cisplatin and selected reagents (acetamide, dimethylacetamide, urea and thiourea) were prepared from research grade commercial products, solubilized in water (LC–MS grade) at a final concentration of ca. 10^{-3} M. In order to favor the aquation reaction, which is a key step in cisplatin activation [36], the cisplatin solution was allowed to stand for one night. Subsequently, the cisplatin solution was mixed with the one of the selected ligand and diluted in H_2O/MeOH 1:1 to a concentration of ca. $5{\cdot}10^{-5}$ M.

2.2. MS and IRMPD spectroscopy

The assayed complexes were investigated using two experimental platforms in order to obtain information on both the fingerprint region of the IR spectrum (800-2000 cm^{-1}) and the XH (X=C, N, O) stretching region (2800-3750 cm^{-1}). In both cases the mass spectrometer unit was equipped with an ESI source of comparable structure and performance. Typical ESI conditions were a flow rate of 180 μL h^{-1}, capillary spray voltage at -4.5 kV, nebulizer at 11 psi, drying gas flow at 6 l min^{-1} and drying gas temperature of 300 °C. IRMPD experiments in the 800-2000 cm^{-1} frequency range have been performed using the free-electron laser (FEL) beamline of the Centre Laser Infrarouge d'Orsay (CLIO). The experiments rely on the coupling of the FEL beamline (operated at 44 MeV for the present experiments) with a hybrid Fourier transform ion cyclotron resonance (FT-ICR) tandem mass spectrometer (APEX-Qe Bruker Daltonics) [37], equipped with a 7.0 T actively shielded magnet and a quadrupole – hexapole interface which permits to mass-filter and accumulate ions prior to irradiation. The mass selected ions were irradiated for 180 to 300 ms with the IR FEL light operating at a repetition rate of 25 Hz and the photofragmentation products were mass analyzed. The 2800-3750 cm^{-1} frequency region of the spectrum was explored using an optical parametric oscillator/amplifier (OPO/OPA) (LaserVision) laser system pumped by a non seeded Nd:YAG laser (Continuum Surelite II). The laser system is coupled to a Paul ion trap mass spectrometer (Esquire 6000+, Bruker Daltonics) in which the ions were mass selected, trapped for 5 to 10 ms, and irradiated for a time ranging from 500 ms to 2 s [38,39], depending on their ease to undergo fragmentation. The output energy from the OPO/OPA laser was ca. 14 mJ/pulse and spectral width 3-4 cm^{-1}. IR spectra are obtained by plotting the photofragmentation yield $R = -\log(I_p/(I_p + \Sigma I_f))$, where I_p and ΣI_f are the integrated intensities of the parent and sum of the fragment ions, respectively, as a function of the photon energy [40].

2.3. Computational details

DFT calculations were employed to obtain optimized structures and thermodynamic data of the complexes dealt with in the present work and to simulate their IR spectra. Plausible starting geometries were selected along the lines of previous work on similar complexes [30]. For geometry optimization and vibrational frequency calculations of the sampled structures the hybrid B3LYP functional was used in conjunction with a polarized basis set system considered large enough to obtain a good description of the structures and vibrational features of the complexes [29,30,41]. In particular we employed the 6-311+G(d,p) basis set for the light atoms and the LanL2TZ effective core potential (ECP) which contains the LANL2 relativistic ECP of Hay and Wadt and a flexible triple-zeta basis set [42] for the platinum atom. The use of an ECP is required to obtain a good description of the core electrons of Pt, given that relativistic effects have been proven relevant for an accurate description of heavy atoms such as platinum [43]. In order to take into better account the contribution of non-covalent interactions, the long-range and dispersion corrected functional ωB97X-D was also employed, maintaining the already reported basis set for both optimization of stationary points and vibrational analysis. In the forthcoming discussion of computational results, spectroscopic data and relative energies will be referred to as obtained at the B3LYP and ωB97X-D levels, respectively. Calculated IR frequencies are scaled by a factor of 0.974 and 0.957 in the fingerprint and XH (X=C, N, O) stretching regions, respectively. All calculations were performed using the Gaussian09 rev. D01 suite of programs [44].

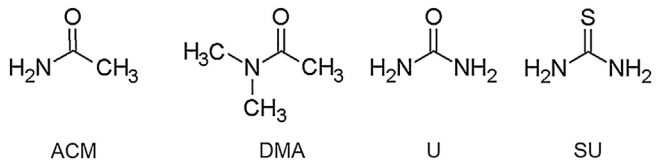

Scheme 1. Structures of acetamide (ACM), dimethylacetamide (DMA), urea (U) and thiourea (SU).

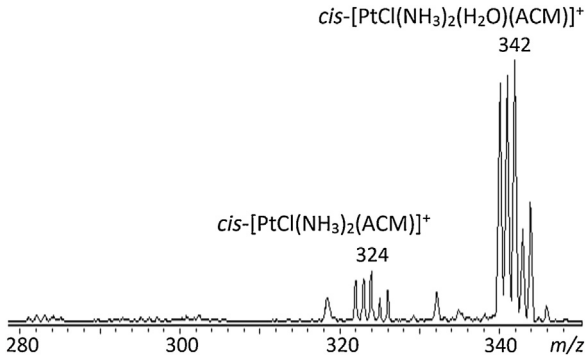

Fig. 1. ESI mass spectrum of a cisplatin-ACM solution. The isotope pattern at *m/z* 322–326 correspond to *cis*-$[PtCl(NH_3)_2(ACM)]^+$, while *cis*-$[PtCl(NH_3)_2(H_2O)(ACM)]^+$ accounts for the isotope pattern at.*m/z*340–344.

3. Results and discussion

3.1. ESI-MS of cisplatin/ligand solutions

Cisplatin has been allowed to react with a selected ligand (L), i.e. acetamide (ACM), dimethylacetamide (DMA), urea (U) and thiourea (SU), depicted in Scheme 1. The formation of a ligand substitution complex is clearly revealed using ESI mass spectrometry, a widely exploited tool for probing cisplatin-derived complexes [21,22,45–49]. The entering ligand has formally displaced a chloride ion, likely via the intermediacy of an aqua complex. The latter species is barely visible at *m/z* 281–285 in the ESI mass spectrum reported in Fig. 1, showing the ion population detected in the presence of ACM as ligand. Major ions correspond to the four-coordinate substitution complex, *cis*-$[PtCl(NH_3)_2(L)]^+$. The *cis*-geometry of *cis*-$[PtCl(NH_3)_2(L)]^+$ substitution complexes conforms to the typically stereoretentive reactions of square planar Pt^{II} complexes [31]. This notion is also confirmed in our previous work where *cis*-$[PtCl_2(NH_3)_2]$ and *trans*-$[PtCl_2(NH_3)_2]$ were allowed to undergo substitution reactions in solution, yielding charged complexes structurally characterized in the gas phase [23,24,28], just the same experimental protocol followed in the present contribution. In addition, a formal five-coordinate complex, *cis*-$[PtCl(NH_3)_2(H_2O)(L)]^+$ is observed. The latter species, presenting an 18 Da higher *m/z* value, is missing in the mass spectrum when SU is the reagent ligand. The isotopic patterns are consistent with the presence of one platinum and one chlorine atom and henceforth the *m/z* value of the lightest ion in the cluster will be reported (i. e. the species containing ^{194}Pt and ^{35}Cl).

The presence of *cis*-$[PtCl(NH_3)_2(H_2O)(L)]^+$ confirms the previous evidence obtained about formal five-coordinate complexes still retaining a water molecule, as already reported in a survey of the reactivity behavior of cisplatin with simple models of its biological targets (i.e. pyridine, 4-methylimidazole and trimethylphosphate) [30]. The absence of any *cis*-$[PtCl(NH_3)_2(H_2O)(SU)]^+$ adduct is not unexpected, though, since the addition of thioanisole, another sulfur-containing nucleophile, to a cisplatin solution did not yield the formally five-coordinate complex, using quite comparable experimental conditions [30]. The *cis*-$[PtCl(NH_3)_2(H_2O)(L)]^+$ complexes delivered by ESI were activated towards both collisionally induced dissociation (CID) and IR multiple photon dissociation (IRMPD). The two activation methods show a comparable fragmentation pattern which involves two dissociation channels. Either water loss is observed or cleavage of the organic ligand, as reported for the *cis*-$[PtCl(NH_3)_2(H_2O)(ACM)]^+$ complex in Fig. 2.

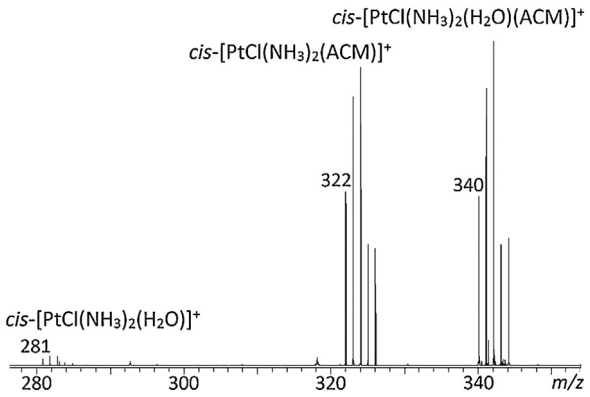

Fig. 2. ESI-MS^2 obtained upon CID of *cis*-$[PtCl(NH_3)_2(H_2O)(ACM)]^+$ at *m/z* 340. The two observed fragmentation channels correspond to water loss (*m/z* 322) and ACM loss (*m/z* 281).

The ratio between the two dissociation paths is similar for the three sampled species (*cis*-$[PtCl(NH_3)_2(H_2O)(L)]^+$, L = ACM, DMA, U) showing largely predominant water loss. In fact, the dehydration channel represents 94 ± 2% of the total fragment ion abundance, under either IRMPD or CID. Both families of complexes, containing either four or five ligands, were submitted to IRMPD spectroscopy varying the photon energy in the fingerprint (800 – 2000 cm^{-1}) and in the XH (X=C, N, O) stretching region (2800-3750 cm^{-1}) in order to unveil their vibrational and structural features.

3.2. Structural features of cis-$[PtCl(NH_3)_2(L)]^+$ complexes

Cisplatin derived complexes, where a chloro ligand has been formally replaced by a simple molecule, mimicking biomolecular functionalities, have been assayed using IRMPD spectroscopy in the mid-IR region. Ion spectroscopy permits to obtain the vibrational features of the sampled ion, allowing to correlate them with characteristic structural motifs [50–56]. The selected ligands, in fact, present two binding sites that may compete for platination, namely the amino nitrogen and the carbonyl group (thiocarbonyl in the case of SU). A computational survey has permitted to identify the most stable structures of the two possible isomers for the four sampled complexes. Geometries and free energies of the optimized structures calculated using both B3LYP and ωB97X-D functionals are reported in Fig. 3, while a complete list of thermodynamic data is reported in Table S1 of the supplementary data (SD).

For the whole set of ligands, the N-bound complexes (**ACM_2**, **DMA_2**, **U_2** and **SU_2**) are higher in energy than their isomers, either O-bound (**ACM_1**, **DMA_1** and **U_1**) or S-bound (**SU_1**). Furthermore, the geometries are fairly similar in each series showing an interaction between the chloro ligand and a hydrogen atom of the amido group in the (S-)O-bound isomers (with the obvious exception of **DMA_1**) and the presence of a hydrogen bond involving an ammonia molecule *cis* to the organic ligand and the (thio)carbonyl moiety in the N-ligated isomers. However, the energy gap between the two families of isomers is notably different moving from ACM to SU, showing a distinct effect exerted by the specific nature of the various ligands. For example, **DMA_2** is 49.7 kJ mol^{-1} higher in free energy relative to **DMA_1**, while **ACM_1** is only 36.6 kJ mol^{-1} lower than **ACM_2**. This difference in relative energy suggests that the electron donating property of the two

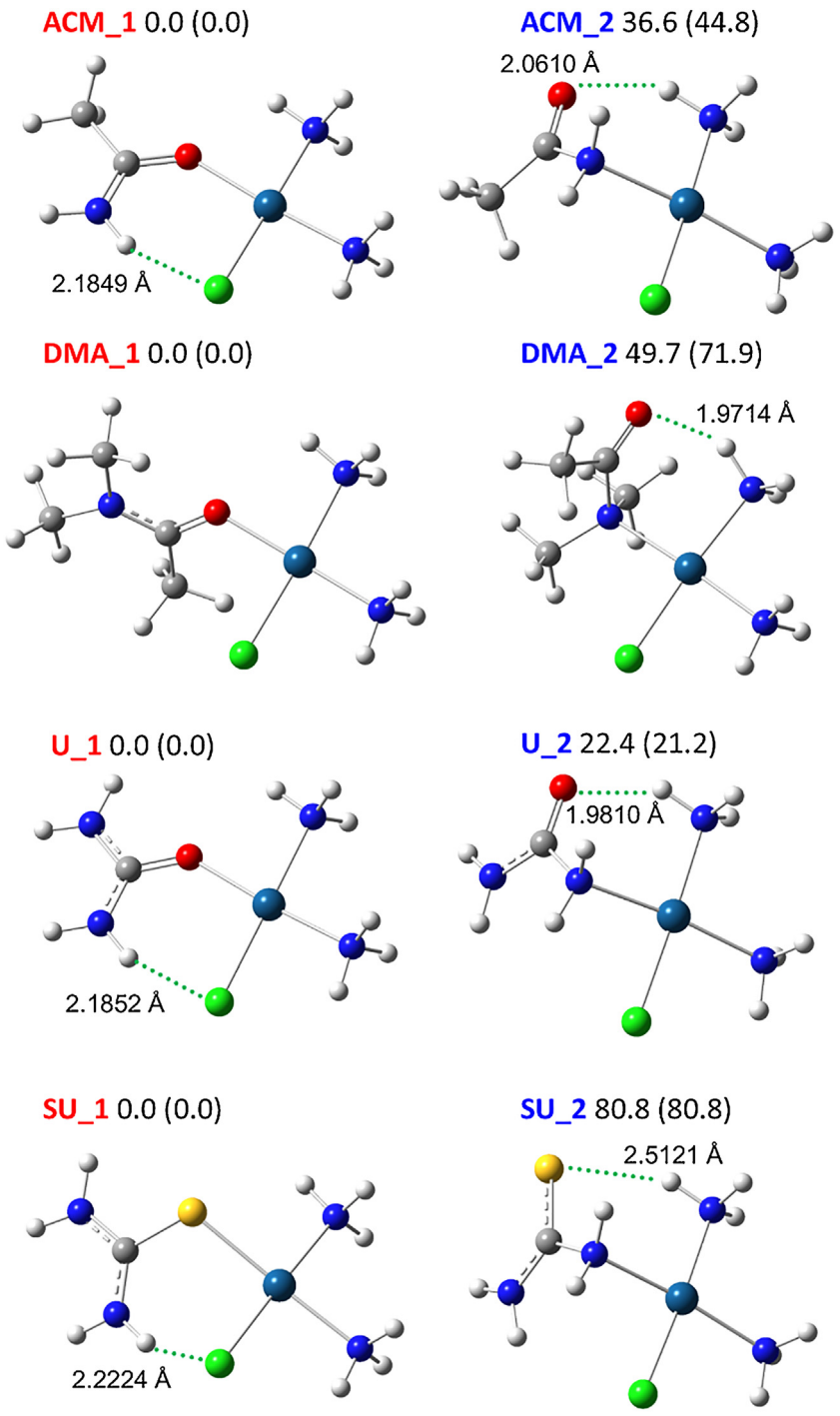

Fig. 3. Optimized geometries of *cis*-$[PtCl(NH_3)_2(L)]^+$ complexes at B3LYP/6-311+G(d,p) (LanL2TZ for Pt) level of theory. Relative free energies as calculated at the ωB97X-D and B3LYP (in brackets) level at 298 K are given in kJ mol^{-1}.

methyl groups in DMA affords a more pronounced stabilizing effect when the carbonyl group is the ligation site rather than in the N-bound complex. However, some influence of steric encumbrance, due to the presence of the methyl groups on the Pt-bound nitrogen atom in **DMA_2** cannot be discarded. One may also notice an important effect when sulfur in SU replaces oxygen in the U ligand. In fact, while the difference in energy between **U_1** and **U_2** is 22.4 kJ mol^{-1}, which is the smallest in the reported series of complexes, the presence of the thiocarbonyl group increases the relative energy of **SU_2** to 80.8 kJ mol^{-1} with respect to **SU_1**. This finding is in line with the well known affinity of "soft" platinum(II) for sulfur donor ligands [57]. However, mere consideration of thermodynamic data may not be adequate to interpret an ion population generated by ESI. It is in fact not unusual to find that high lying isomers, preferentially formed in solution, may be kinetically trapped in the gas-phase [29,30,58,59].

Vibrational frequency analysis has been performed on the geometries reported in Fig. 3 and calculated IR spectra are compared with the IRMPD spectra of *cis*-$[PtCl(NH_3)_2(L)]^+$ ions (Fig. 4 and Table S2 in the SD) in order to obtain structural information. When submitted to resonant IR photons the earliest dissociation channel is ammonia loss, followed by HCl loss. Only a small per-

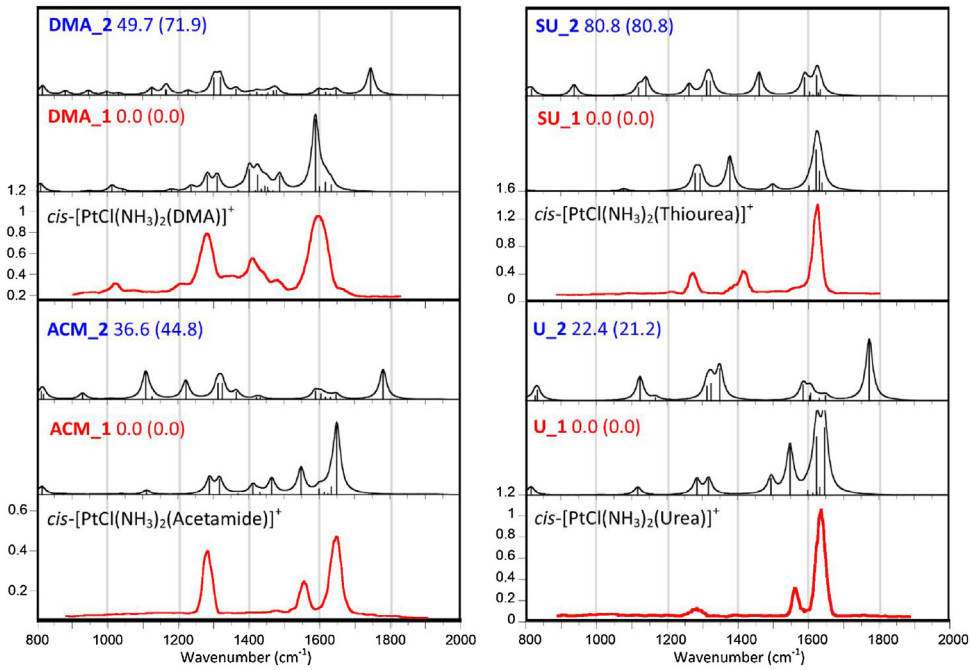

Fig. 4. IRMPD spectra (red profiles) of *cis*-[PtCl(NH_3)$_2$(L)]$^+$ (L = ACM, DMA, U, TU) compared with the IR spectra (black profiles) calculated at B3LYP/6-311+G(d,p) level for the isomers reported in Fig. 3. Theoretical harmonic frequencies are scaled by a factor of 0.974. Relative free energies at 298 K are in kJ mol^{-1}, as calculated at the ωB97X-D and B3LYP (in brackets) level.

centage of L loss (comprised between the 3% and 6% of the total product ion abundance) is observed in the case of ACM, DMA and U complexes, while no [PtCl(NH_3)$_2$]$^+$ fragment is ever generated from the *cis*-[PtCl(NH_3)$_2$(SU)]$^+$ complex, in agreement with the expected stronger binding of platinum to the thiocarbonyl group when compared to carbonyl. IRMPD mass spectra are reported in Fig. S1 in the SD. The comparison of theoretical and experimental spectra depicted in Fig. 4 supports metal coordination to the carbonyl (or thiocarbonyl) group rather than to the amino group. In this regard, the lack of any band for free C=O stretching in the IRMPD spectra of the ACM, DMA and U complexes, calculated at 1781, 1745 and 1772 cm^{-1} for **ACM_2**, **DMA_2** and **U_2**, respectively, speaks against any significant contribution of N-bound isomers in the sampled population. In addition, a few vibrational features deserve to be highlighted. Three main features are present in the experimental spectrum of *cis*-[PtCl(NH_3)$_2$(ACM)]$^+$. All of them are well accounted for by the **ACM_1** calculated frequencies confirming the O-bound isomers to form the major part of the gas-phase population. The band at 1646 cm^{-1} can be interpreted as the scissor-like bending of NH_2 which was calculated for **ACM_1** at 1650 cm^{-1}, while the band at 1559 cm^{-1} is consistent with a vibrational motion of **ACM_1** calculated at 1548 cm^{-1}, wherein the scissoring mode of the amino group is coupled with CO stretching. The pronounced feature at 1281 cm^{-1} is associated with a convolution of umbrella modes of the ammonia molecules in the coordination sphere of platinum, calculated at 1289 and 1318 cm^{-1}. Finally, the barely visible signal at 1475 cm^{-1} is accounted for by the CH_3 umbrella mode of **ACM_1** expected at 1465 cm^{-1}.

Moving to *cis*-[PtCl(NH_3)$_2$(DMA)]$^+$, the calculated spectrum of the O-bound isomer **DMA_1** is in good agreement with the experimental IRMPD features. Indeed, the IRMDP spectrum of the DMA adduct is quite similar to the one of *cis*-[PtCl(NH_3)$_2$(ACM)]$^+$, although some bands just fortuitously coincide and have a different interpretation. For example, the band at 1596 cm^{-1} consistent with the CN stretching of **DMA_1** (1589 cm^{-1}) appears in the same region as the NH_2 scissoring modes. The set of signals in the region 1400-1500 cm^{-1} of the IRMPD spectrum is well reproduced by the calculated umbrella modes of the methyl groups of DMA at 1402 and 1425 cm^{-1} and by the CO stretching coupled with CH_3 asymmetric bendings at 1488 cm^{-1} of **DMA_1**, while the asymmetric bending mode of CH_3 (1014 cm^{-1}) accounts for the IRMPD signal at 1020 cm^{-1}. At 1280 cm^{-1} the second highest experimental band is consistent with a convolution of the two umbrella modes of the ammonia, as already reported for *cis*-[PtCl(NH_3)$_2$(ACM)]$^+$, which are calculated for **DMA_1** at 1283 and 1312 cm^{-1}. The last species presenting a carbonyl group, *cis*-[PtCl(NH_3)$_2$(U)]$^+$, shows a similar pattern as the ACM complex. The only difference obviously pertains to the presence of two NH_2 groups, which are spectroscopically different due to the interaction of one of them with the chloro ligand (geometries are depicted in Fig. 3). Therefore, two slightly different scissoring modes are calculated for the most stable isomer **U_1** at 1624 and 1646 cm^{-1} in agreement with the experimental band at 1625 cm^{-1}. Also other IRMPD bands are well reproduced by the calculated IR spectrum of the O-bound isomer **U_1** which accounts for the experimental signals at 1560 and 1280 cm^{-1} by the CO stretching mode associated to NH_2 scissoring at 1548 cm^{-1} and by the umbrella modes of ammonia at 1285 and 1318 cm^{-1}, respectively.

The comparison of the vibrational features of *cis*-[PtCl(NH_3)$_2$(SU)]$^+$ with the calculated IR spectra of the S-bound isomer **SU_1** and the N-bound one **SU_2** is instead less straightforward. While the calculated modes of **SU_1** well interpret the experimental signatures, there are no evident spectroscopic indications that allow to discard the presence of the **SU_2** isomer, as was the case of the diagnostic C=O stretching that was missing in the spectra of the previous complexes. However, the sharpness of the band at 1627 cm^{-1} is better simulated by the NH_2 scissoring modes of **SU_1** which are calculated at 1623 and 1632 cm^{-1} than by the more widely parted ones of **SU_2** at 1625 and 1590 cm^{-1}. In the calculated normal modes of **SU_2**, in fact, one bending mode is red-shifted due to the binding of the corresponding amino group to platinum. In addition, the bands at 1417 and 1280 cm^{-1} are in fair agreement with the CS stretching coupled with the NH_2 scissoring at 1378 cm^{-1} and the umbrella modes of the ammonia at 1280 and 1294 cm^{-1}, respectively, of **SU_1**.

3.3. Structural features of cis-[PtCl(NH_3)$_2$(H_2O)(L)]$^+$ complexes

When cisplatin is allowed to react with ACM, DMA and U, ESI mass spectra show the presence of formally five-coordinate complexes presenting the general formula [PtCl(NH_3)$_2$(H_2O)(L)]$^+$ (L = ACM, DMA and U). Understanding the coordination environment of platinum and the position of the fifth ligand is crucial to interpret the reactivity of the complexes. In this regard, one may conceive the formation of a platinum complex presenting five metal-ligand bonds. However, in this option any kind of geometrical arrangement of positively charged Pt^{II} complexes fails to lie in an energy minimum in spite of careful search, rather leading to the structure of a non-covalently bound complex where one of the ligands is placed in external coordination [30]. In particular, two plausible isomers may possess either a covalently bound water and external L (represented as {*cis*-[PtCl(NH_3)$_2$(H_2O)]$^+$ · L}) or inner sphere L and water solvating the complex ({*cis*-[PtCl(NH_3)$_2$(L)]$^+$ · H_2O}). The observed fragmentation pattern involves loss of both water and L with the former channel largely predominant, as shown in Fig. 2 and Fig. S2 of the SD. However, the major loss of water should not be taken as evidence in favor of non-covalently bound water [30]. IRMPD spectroscopy is then used to discriminate between the two possible isomers. It is important to note that both photofragmentation processes, involving either water or L ligand loss, are uniformly represented all along the IRMPD spectra recorded in the spanned wavenumber ranges, as shown in Fig. S2. This finding supports the presence of a common ion population, against the supposition that water loss might sample {[PtCl(NH_3)$_2$L]$^+$ · H_2O} complexes while ligand loss might selectively sample {([PtCl(NH_3)$_2$(H_2O)]$^+$ · L} complexes. Thermodynamic data are collected in Table S1 of the SD while vibrational modes and corresponding frequencies are reported in Table S3 of the SD.

3.3.1. Cis-[PtCl(NH_3)$_2$(H_2O)(L)]$^+$ complexes (L = ACM)

Fig. 5 presents the IRMPD spectrum of *cis*-[PtCl(NH_3)$_2$(H_2O)(ACM)]$^+$ (red profile) compared with the theoretical IR spectra of the lowest lying conformers pertaining to the two families of possible isomers, which are gathered by colors, either orange for {[PtCl(NH_3)$_2$L]$^+$ · H_2O} (indicated by the ACM-H2O notation) or blue for {([PtCl(NH_3)$_2$(H_2O)]$^+$ · L} (indicated by the H2O-ACM notation).

The global minimum is **ACM-H2O_1**. In this conformer the water molecule interacts by hydrogen bonds with the two ammonia ligands and the platinum complex presents a structure resembling closely **ACM_1** (Fig. 3). Other species in this family of isomers are higher in free energy. **ACM-H2O_2** at 6.9 kJ mol^{-1} holds the external water between chloro and ammonia ligands while **ACM-H2O_3** at 11.2 kJ mol^{-1} loses the stabilizing interaction between the amido NH_2 and Cl because the methyl group is now oriented towards the chloro ligand.

The lowest lying species in the family of complexes holding ACM in external position to the cisplatin complex is **H2O-ACM_1**, lying at 24.7 kJ mol^{-1} relative to **ACM-H2O_1**. In this geometry the carbonyl group of ACM acts as hydrogen bond acceptor for the inner sphere aqua ligand and a hydrogen bond interaction also binds the amido NH_2 to the chloro ligand. This latter bonding is instead lost in **H2O-ACM_2**, because the amido group is oriented far away from Cl and the free energy of this complex is 28.4 kJ mol^{-1} relative to the global minimum. Conformer **H2O-ACM_3**, lying at 28.5 kJ mol^{-1}, shows instead a bisected interaction of the carbonyl oxygen with both water and ammonia ligands of platinum. Other calculated structures, are presented in Fig. S3 of the SD. Thermodynamic data, therefore, suggest a major participation of {[PtCl(NH_3)$_2$L]$^+$ · H_2O} complexes in the sampled gas-phase population. However, critical evaluation is required due to the nature of the experiment and to the fact we are comparing isomeric families which are not likely to interconvert in the gas-phase.

Structural information is gained from the IRMPD spectrum presented in Fig. 5 displaying several features in both the fingerprint and XH stretching regions, in high photofragmentation yield. However, most of the signals are shared by species pertaining to both families of isomers (either {[PtCl(NH_3)$_2$L]$^+$ · H_2O} or {([PtCl(NH_3)$_2$(H_2O)]$^+$ · L}). Notably, the absence of a band in the 3650-3750 cm^{-1} region of the experimental spectrum in Fig. 5 allows to assign the major part of the sampled population to the {([PtCl(NH_3)$_2$(H_2O)]$^+$ · L} isomer. In fact, all isomers presenting a solvating water molecule show a diagnostic band associated to the asymmetric stretching of water, calculated at 3707, 3733 and 3708 cm^{-1} for **ACM-H2O_1**, **ACM-H2O_2**, **ACM-H2O_3**, respectively. Therefore, this family of isomers will not be further considered in the forthcoming interpretation of the experimental spectrum. The IRMPD spectrum of *cis*-[PtCl(NH_3)$_2$(ACM)(H_2O)]$^+$ (Fig. 5) shows a number of signals in the NH and OH stretching region, suggesting the presence of multiple structural arrangements. Thus, in the 3500-3650 cm^{-1} region, the band at 3613 cm^{-1} can be assigned to the OH stretching of the water ligand calculated at 3641 cm^{-1} for both **H2O-ACM_1** and **H2O-ACM_2**. A shoulder is also present at 3585 cm^{-1} compatible with the OH stretching of water for **H2O-ACM_3**, calculated at 3614 cm^{-1}. The 30 cm^{-1} discrepancy between experimental and calculated frequencies was already noted in similar complexes [30]. Further on, two intense signals at 3561 and 3532 cm^{-1} are in agreement with the NH_2 asymmetric stretch calculated at 3550/3547 and 3517 cm^{-1} for **H2O-ACM_2**/**H2O-ACM_3** and **H2O-ACM_1**, respectively, thus confirming the presence of at least the three species contributing to the sampled ions population.

At 3441 cm^{-1} the spectrum presents an important feature ascribed to the symmetric stretching of the amido NH_2, calculated at 3426 and 3428 cm^{-1} for **H2O-ACM_2** and **H2O-ACM_3**, respectively. Regarding **H2O-ACM_1**, this mode is red-shifted to 3335 cm^{-1} due to interaction between the amido NH_2 and the chloro ligand, thus falling in a rather congested region of the IRMPD spectrum and likely responsible for the shoulder at ca. 3322 cm^{-1} of a broad absorption with main signals at 3389 and 3354 cm^{-1} due to asymmetric stretching of the ammonia molecules. In the 2800-3300 cm^{-1} region of the experimental spectrum there appears broad, smeared IRMPD activity, in particular a wide feature at 3228 cm^{-1} is consistent with the NH stretching of the ammonia interacting with the carbonyl group of ACM within **H2O-ACM_3** (calculated 3219 cm^{-1}).

In the fingerprint region, the IRMPD spectrum shows several bands assigned to the combined contribution of **H2O-ACM_1**, **H2O-ACM_2**, and **H2O-ACM_3**, as illustrated in detail in Table S3 of the SD. The major bands are mentioned here. An important feature at 1660 cm^{-1} followed by a shoulder at 1637 cm^{-1} can be attributed to the CO stretching coupled with H_2O bending of **H2O-ACM_3** (1657 cm^{-1}) and with NH_2 "scissor-like" bendings, calculated at 1633, 1637 and 1641 cm^{-1} for **H2O-ACM_1**, **H2O-ACM_2** and **H2O-ACM_3**, respectively. The maximum at 1587 cm^{-1} is in good agreement with the amide C=O stretching red-shifted by the interaction with the water molecule coordinated to platinum (calculated at 1575, 1579 and 1575 cm^{-1} for **H2O-ACM_1**, **H2O-ACM_2** and **H2O-ACM_3**, respectively). The symmetric bending of ammonia "umbrella" mode calculated around 1315 cm^{-1} for all three species, may account for the band at 1297 cm^{-1} of noticeably high intensity in the IRMPD spectrum.

3.3.2. Cis-[PtCl(NH_3)$_2$(H_2O)(L)]$^+$ complexes (L = DMA)

The IRMPD spectrum of the *cis*-[PtCl(NH_3)$_2$(H_2O)(DMA)]$^+$ complex is presented in Fig. 6 together with the calculated IR spectra of the lowest lying species, conforming to either {[PtCl(NH_3)$_2$L]$^+$ · H_2O} (such as **DMA-H2O_1**) or {([PtCl(NH_3)$_2$(H_2O)]$^+$ · L}, such as

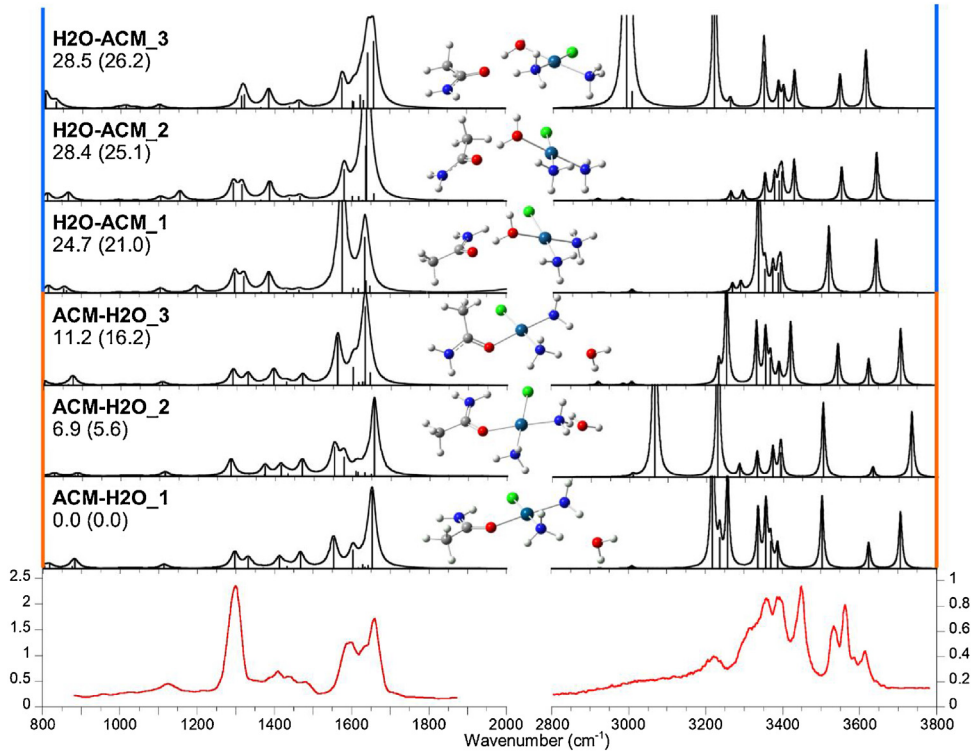

Fig. 5. IRMPD spectrum of *cis*-[PtCl(NH_3)$_2$ (H_2O)(ACM)]$^+$ (red profile) compared with the theoretical IR spectra of **ACM-H2O_1**, **ACM-H2O_2**, **ACM-H2O_3**, **H2O-ACM_1**, **H2O-ACM_2** and **H2O-ACM_3**. Optimized geometries at the B3LYP/6-311+G(d,p) level are reported together with relative free energies at the ωB97X-D and B3LYP (in bracket) levels at 298 K in kJ mol^{-1}.

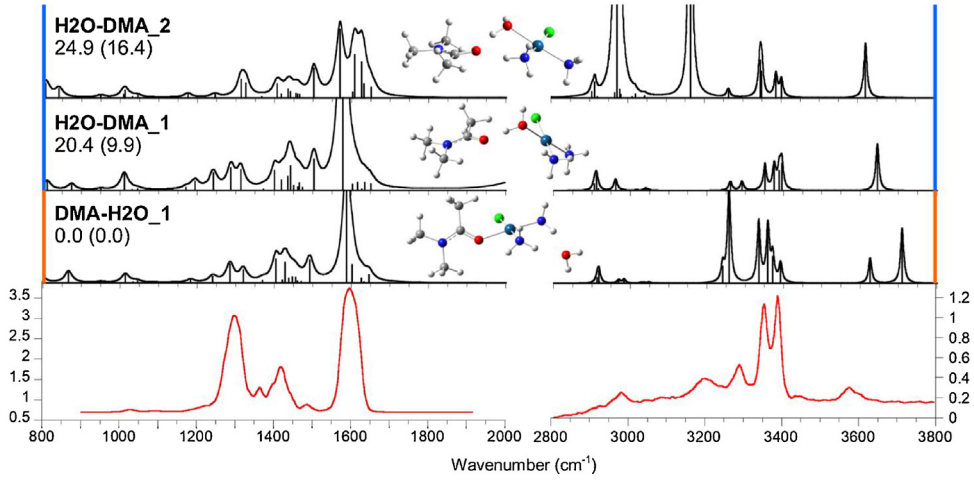

Fig. 6. IRMPD spectrum of *cis*-[PtCl(NH_3)$_2$(H_2O)(DMA)]$^+$ (red profile) compared with the theoretical IR spectra of **DMA-H2O_1**, **H2O-DMA_1** and **H2O-DMA_2**. Optimized geometries at the B3LYP/6-311+G(d,p) level are reported together with relative free energies at the ωB97X-D and B3LYP (in bracket) levels at 298 K in kJ mol^{-1}.

H2O-DMA_1 and **H2O-DMA_2**). Higher energy structures are presented in Fig. S4 of the SD.

The XH (X=C, N, O) stretching region is once again critical to distinguish between the adducts with either DMA or water outside the coordination sphere of platinum. In particular, the IRMPD spectrum lacks a signal for the asymmetric stretching of free water, calculated at 3709 cm^{-1} for **DMA-H2O_1**. On the contrary, the experimental spectrum presents a feature at 3573 cm^{-1} with a slope around 3600 cm^{-1} consistent with the presence in the sampled population of the two lowest lying conformers generated by the interaction of the aqua complex of cisplatin with DMA (**H2O-DMA_1** and **H2O-DMA_2**). In fact, the OH stretching vibration calculated for the two species is slightly different, 3645 and 3620 cm^{-1} for **H2O-DMA_1** and **H2O-DMA_2**, respectively, thus suggesting a contribution of both. At lower frequency in the 2800-3500 cm^{-1} region, asymmetric stretching modes of the ammonia molecule are calculated at 3395, 3388, 3375 and 3351 cm^{-1} for **H2O-DMA_1**, and at 3400, 3386, 3349 and 3345 cm^{-1} for **H2O-DMA_2**, accounting also for the major peaks observed at 3389 and 3352 cm^{-1}. Symmetric stretching modes of ammonia ligands which are not involved in hydrogen bonding are calculated at 3291 and 3260 cm^{-1} for **H2O-DMA_1**, and 3262 cm^{-1} for **H2O-DMA_2** in agreement with the experimental band at 3290 cm^{-1}. In the second conformer however, one ammonia molecule is engaged in hydrogen bonding with the carbonyl group of DMA, causing a red-shift to 3162 cm^{-1}, which is consistent with the broad experimental feature at 3200 cm^{-1}. Finally, a signal

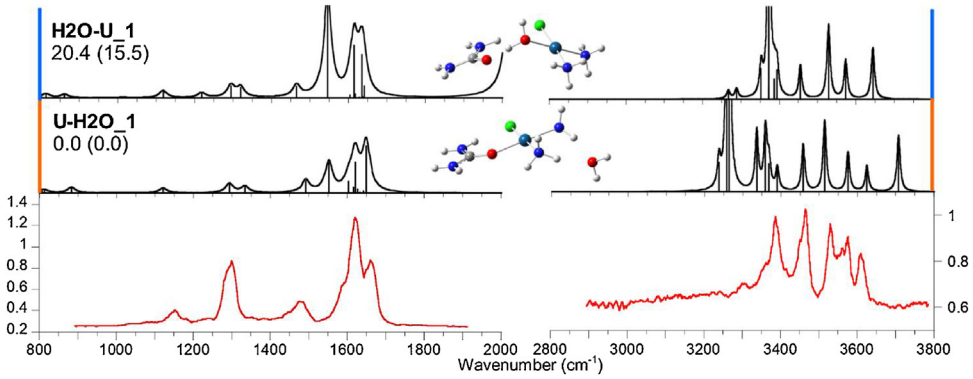

Fig. 7. IRMPD spectrum of *cis*-$[PtCl(NH_3)_2(H_2O)(U)]^+$ (red profile) compared with the theoretical IR spectra of **U-H2O_1** and **H2O-U_1**. Optimized geometries at the B3LYP/6-311+G(d,p) level are reported together with relative free energies at the ωB97X-D and B3LYP (in bracket) levels at 298 K in kJ mol^{-1}.

at 2978 cm^{-1} can be attributed to the OH stretching involved in the interaction with the carbonyl group in the **H2O-DMA_2** geometry (calculated 2972 cm^{-1}).

The fingerprint region of the IRMPD spectrum is dominated by a broad band centered at 1597 cm^{-1}, expression of the presence of multiple absorptions in this range. In particular, at 1577 cm^{-1} an intense CN stretching coupled with CO stretch is calculated for **H2O-DMA_1**, while **H2O-DMA_2** presents three vibrational modes related to H_2O scissoring coupled with NH_3 bend at 1624 cm^{-1}, CO stretching at 1607 cm^{-1} and CN stretching at 1569 cm^{-1}, respectively. A broad absorption at 1417 cm^{-1}can be attributed to a convolution of CH_3 umbrella modes calculated at 1441, 1418 and 1400 cm^{-1} for **H2O-DMA_1**, and 1434, 1416 and 1406 cm^{-1} for **H2O-DMA_2**, while the pronounced band at 1295 cm^{-1} is ascribed to umbrella modes of the ammonia calculated at 1312/1287 and 1324/1312 cm^{-1} for **H2O-DMA_1** and **H2O-DMA_2**, respectively.

3.3.3. Cis-*[PtCl(NH$_3$)$_2$(H$_2$O)(L)]$^+$ complexes (L = U)*

The IRMPD spectrum *cis*-$[PtCl(NH_3)_2(H_2O)(U)]^+$ is reported in Fig. 7. The experiment is compared with the IR spectra of the lowest lying conformers from the two families of isomers already discussed. Other calculated structures are presented in Fig. S5 of the SD.

H2O-U_1, presenting urea in an external hydrogen bond interaction with the inner water ligand, is 20.4 kJ mol^{-1} higher in energy relative to the **U-H2O_1** isomer where water is solvating the square-planar complex *cis*-$[PtCl(NH_3)_2(U)]^+$ complex. In spite of **U-H2O_1** being the global energetic minimum, as already observed in the ACM and DMA cases, the IRMPD spectrum rather supports the presence of an adduct between an aqua platinum(II) complex and an external U molecule. In this regards, particularly diagnostic is the absence of an absorption around 3708 cm^{-1}, the calculated asymmetric water stretching of **U-H2O_1**. Moreover, the calculated IR spectrum of the **H2O-U_1** isomer is in fair agreement with the experimental one as shown in Fig. 7. In particular, the 2800-3800 cm^{-1} region of the IR spectrum is well interpreted although the experimental band at 3607 cm^{-1} is assigned to the OH stretching of water calculated at a somewhat higher frequency (3644 cm^{-1}). IRMPD bands at 3574 and 3526 cm^{-1} are consistent with the asymmetric stretching of free NH_2 at 3573 cm^{-1} and of NH_2 interacting with the chloro ligand at 3528 cm^{-1}, respectively. Two other important features in the higher frequency part of the IRMPD spectrum are at 3464 cm^{-1}, consistent with symmetric stretching of NH_2 remote from Cl calculated at 3454 cm^{-1}, and at 3384 cm^{-1}, which is interpreted by the NH_2 symmetric stretching red-shifted by the interaction with Cl (3372 cm^{-1}). In the fingerprint region, a convoluted band comprises two peaks at 1663 and 1620 cm^{-1} and a shoulder at 1580 cm^{-1}. The former signals are consistent with NH_2 scissoring modes calculated at 1634 and 1613 cm^{-1}, while the shoulder can be attributed to the CO stretch of **H2O-U_1**, calculated at 1545 cm^{-1}. This carbonyl stretching mode is considerably red shifted with respect to typical absorbance ranges due to strong hydrogen bonding and coupling with OH stretching and NH_2 rocking motions and likely overestimated in activity by computation.

4. Potential energy surface and concluding remarks

The appraisal of IRMPD features of formally five-coordinate platinum(II) complexes backed by a computational survey of plausible structures concur in ascribing the major part of the ion population to $\{([PtCl(NH_3)_2(H_2O)]^+ \cdot L\}$ isomers. However, these species are higher in energy than their counterparts presenting water outside the first coordination sphere of platinum. Exploring the potential energy surface (PES) for the reaction between the aqua complex of cisplatin and the inspected ligands can shed light on the reasons beneath the bias between the experimental conformational sampling provided by IRMPD spectroscopy and the calculated energies of isomeric complexes. The PES for the formation of the substitution complexes *cis*-$[PtCl(NH_3)_2(L)]^+$, where L = ACM, DMA, U and SU, from the aqua complex and the bare ligand is outlined in Fig. 8. The PES shows a double well profile where the first minimum corresponds to the adduct with externally coordinated L, while the second one contains a species where water is solvating the substitution complex. The second well is lower in energy and therefore it should form the major part of the population if thermal equilibrium was achieved under sampling conditions. Instead, structural analysis by IRMPD spectroscopy showed a different landscape where $\{(cis\text{-}[PtCl(NH_3)_2(H_2O)]^+ \cdot L\}$ is largely predominant, thus suggesting that the experimental setup is able to extract from solution the earliest intermediate in the substitution reaction of the cisplatin aqua complex, the so called encounter complex. As shown in Fig. 8, the energy needed to overcome the transition states and reach the global minima of the PES (67, 70, and 68 kJ mol^{-1} for the reaction with ACM, DMA, and U, respectively) seems, thus, to be higher than the energy imparted to ions in the ESI process and transfer to the ion trap. In the case of thiourea, instead, the activation energy for ligand substitution is much lower (43 kJ mol^{-1}) which may be the reason preventing to observe a *cis*-$[PtCl(NH_3)_2(H_2O)(SU)]^+$ adduct in the mass spectrum.

In addition, the $\{(cis\text{-}[PtCl(NH_3)_2(H_2O)]^+ \cdot SU\}$ complex is the least bound among the sampled species with a dissociation energy of 117 kJ mol^{-1} to be compared with 126, 131, 133 kJ mol^{-1} when L is ACM, DMA, and U, respectively. Alternatively, one may expect to be able to extract and isolate from solution by ESI the complex obtained by ligand substitution *cis*-$[PtCl(NH_3)_2(L)]^+$ still associ-

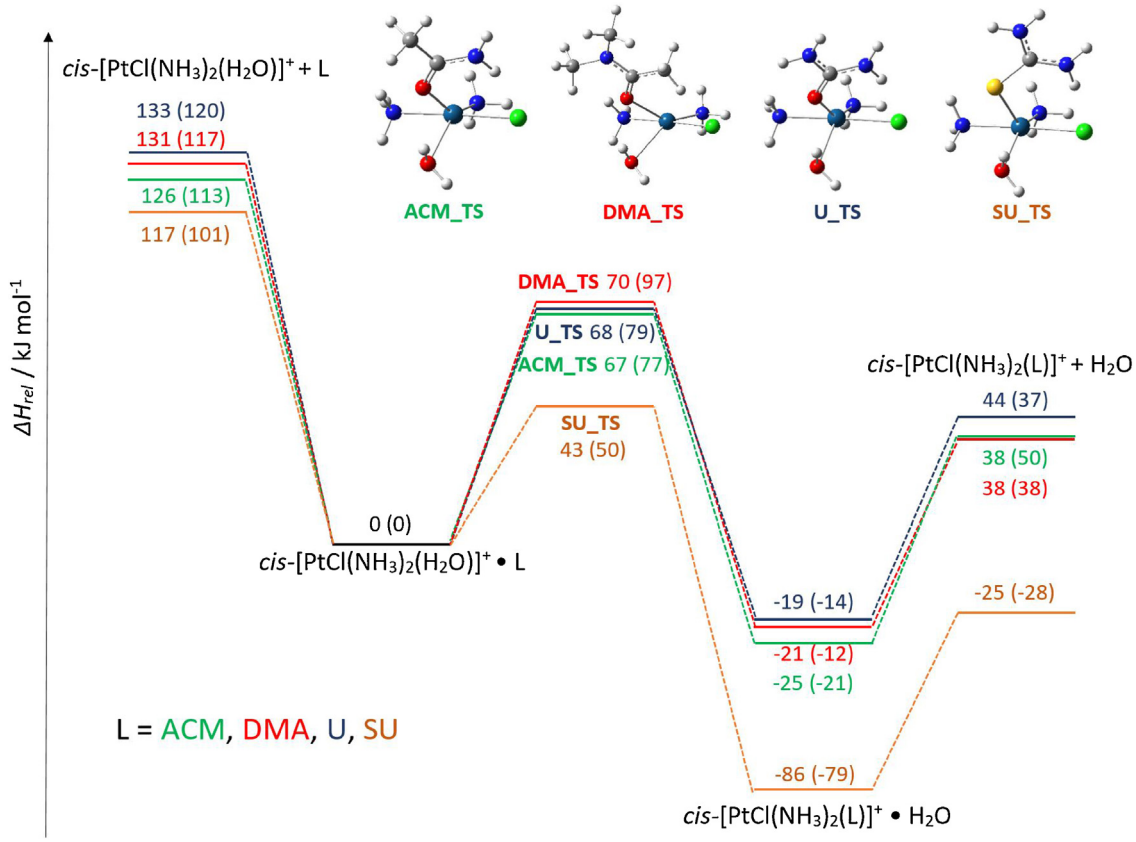

Fig. 8. PES for the reaction of *cis*-$[PtCl(NH_3)_2(H_2O)]^+$ with L (L = ACM, DMA, U and SU). Geometries of the transition states optimized at B3LYP/6-311+G(d,p) are shown. Relative enthalpies (kJ mol^{-1}) are reported at the ωB97X-D/6-311+G(d,p) level. Values at B3LYP/6-311+G(d,p) level are also reported (in brackets).

ated to a water molecule, namely the {(*cis*-$[PtCl(NH_3)_2(L)]^+ \cdot H_2O$} adduct. Indeed, this species is the absolute minimum in the gas phase PES depicted in Fig. 8. However, the low binding energy, ca. 60 kJ mol^{-1}, for the dissociation of water is the likely reason for the failure of ESI in delivering any {(*cis*-$[PtCl(NH_3)_2(L)]^+ \cdot H_2O$} adduct, in spite of the documented presence of $[PtCl(NH_3)_2(L)]^+$ in the sampled water/methanol solution

Finally the branching between L vs. H_2O loss upon activation of *cis*-$[PtCl(NH_3)_2(H_2O)(L)]^+$ complexes can be commented with respect to the difference in activation energy for the two competing processes. This is possible since the parent ions *cis*-$[PtCl(NH_3)_2(H_2O)(L)]^+$ when allowed to absorb tunable IR photons yield both dissociation products in about constant ratio, as reported in Fig. S2, and the branching between L and water loss can be compared with the theoretical data obtained for the PES. A similar branching ratio is observed for the three complexes with a massive predominance of the water loss channel (ca. 96%) in agreement with the difference between the threshold energy for direct ligand dissociation and the activation energy for the ligand displacement process. The observed values of 59, 61, and 65 kJ mol^{-1} for ACM, DMA and U, respectively, are in fact consistent with the predominance of the water loss channel. They are also in good agreement with a previous report regarding the reaction of trimethylphosphate as ligand where the difference in energy of 67 kJ mol^{-1} between the reactants and transition state for substitution led to a comparable dissociation branching ratio (9:91 for ligand versus water loss) [30].

In conclusion, the *cis*-$[PtCl(NH_3)_2(H_2O)(L)]^+$ complexes have been characterized as {(*cis*-$[PtCl(NH_3)_2(H_2O)]^+ \cdot L$} adducts, namely the encounter complex early actor in the ligand substitution mechanism proposed by Eigen and Wilkins for the aqua ligand displacement in metal complexes in solution. The IRMPD process, besides disclosing the structure of the sampled adduct, also activates ligand displacement by vibrational energy deposition, thanks to the lower barrier for reaching the five-coordinate transition state relative to the threshold for back dissociation to *cis*-$[PtCl(NH_3)_2(H_2O)]^+ + L$.

It is appropriate to underline once again that the product adduct, namely {(*cis*-$[PtCl(NH_3)_2(L)]^+ \cdot H_2O$}, is not in fact observed in spite of the recognized presence of *cis*-$[PtCl(NH_3)_2(L)]^+$ in the solution sampled by ESI. Thus, the favorable circumstances allowing detection of {(*cis*-$[PtCl(NH_3)_2(H_2O)]^+ \cdot L$} are (i) a relatively high barrier for back dissociation and (ii) a relatively high activation energy for the ligand substitution step. When the second condition is not met, e. g. in the SU case, no formal five-coordinate adduct is obtained by ESI in the experimental conditions adopted, in spite of efforts tending to optimize soft delivery of ionic species.

By and large, the non-covalent adduct of interest needs to lie in a fairly deep energy well, to allow detection and characterization.

As a final note, the reactivity pattern observed in the present experiments may be viewed in the context of the well established mechanistic landscape regarding ligand substitution reactions of square planar platinum(II) complexes in solution [31]. Extensive studies have been devoted to these kinetically inert species which have allowed defining an effective nucleophilicity scale for various incoming ligands. The process is generally agreed to be associative, involving nucleophilic attack of the entering ligand and passing through a series of five-coordinate transition states and reactive intermediates. However, it is difficult to distinguish between an associative mechanism (A) proceeding through a reactive intermediate of increased coordination number or an associative interchange mechanism (I_a) where bond making is of major importance but there is no discrete intermediate formed [60,61].

Extensive theoretical studies have been carried out describing the reaction of platinum(II) complexes with nucleophiles and the interaction with water. Neutral cisplatin has been envisaged as hydrogen bond acceptor towards H_2O by means of the electron density in the d_z2 orbital [62,63]. Ligand exchange reactions proceeding via a trigonal bipyramidal transition states have been characterized [64–67] and microsolvation effects and base selectivity in cisplatin reactivity have been considered [68]. In particular, the mechanism of water exchange reactions in square planar *trans*-$Pt[(NH_3)_2T(H_2O)]^{n+}$complexes has been reported as involving an associative interchange mechanism [69]. Only in the presence of a T ligand with strong π-back donation ability is a five-coordinate intermediate stabilized so that the substitution reaction proceeds by a two step associative mechanism. In the solid state, a number of pentacoordinated Pt^{II} complexes have been characterized by crystallography, none of them owning the ligation pattern of the presently studied systems [70]. Overall it is tempting to conclude that the suggested mechanism for ligand substitution on square-planar complexes passing through square-pyramidal and trigonal-bipyramidal stages has probably to be re-thought in the light of experimental and computational results, as also reported in the present contribution.

Acknowledgements

This research was supported by Università di Roma "La Sapienza" (DR n. 3210/16), by the European Community's Horizon 2020 Programme (INFRAIA-02-2017, under Grant Agreement No. 731077), and by the French FT-ICR network (FR3624CNRS).

The authors wish to thank J. M. Ortega and the CLIO team and are grateful to D. Scuderi and to V. Steinmetz for their support during the experiments.

References

[1] B. Butschke, H. Schwarz, Mechanistic studies on the gas-phase dehydrogenation of alkanes at cyclometalated platinum complexes, Chem. Eur. J. 18 (2012) 14055–14062.
[2] B. Butschke, H. Schwarz, On the activation of chloromethanes by cyclometalated $[Pt(bipy - H)]^+$ in the gas phase: A mechanistic study, Int. J. Mass Spectrom. 306 (2011) 108–113.
[3] B. Butschke, S.G. Tabrizi, H. Schwarz, Ion-molecule reactions of ŕollover̆cyclometalated $[Pt(bipy-H)]^+$ (bipy = 2,2'-bipyridine) with dimethyl ether in comparison with dimethyl sulfide: An experimental/computational study, Chem. Eur. J. 16 (2010) 3962–3969.
[4] B. Butschke, M. Schlangen, D. Schröder, H. Schwarz, Platinum(II)-mediated dehydrosulfurization and oxidative carbon-carbon coupling in the gas-phase decomposition of thioethers, Int. J. Mass Spectrom. 283 (2009) 3–8.
[5] D. Schröder, H. Schwarz, Gas-phase activation of methane by ligated transition-metal cations, Proc. Natl. Acad. Sci. U. S. A. 105 (2008) 18114–18119.
[6] B. Butschke, H. Schwarz, R̈ollover̆cyclometalation - Early history, recent developments, mechanistic insights and application aspects, Chem. Sci. 3 (2012) 308–326.
[7] K. Koszinowski, D. Schröder, H. Schwarz, Reactions of platinum-carbene clusters $Pt_nCH_2^+$ (n = 1-5) with O_2, CH_4, NH_3, and H_2O: Coupling processes versus carbide formation, Organometallics 22 (2003) 3809–3819.
[8] K. Koszinowski, D. Schröder, H. Schwarz, Reactivity of small cationic platinum clusters, J. Phys. Chem. A 107 (2003) 4999–5006.
[9] D. Schröder, H. Schwarz, C-H and C-C bond activation by bare transition-metal oxide cations in the gas phase, Angew. Chem. Int. Ed. 34 (1995) 1973–1995.
[10] R. Liyanage, M.L. Styles, R.A.J. O'Hair, P.B. Armentrout, Guided ion beam and ab initio studies of platinum chloride cations, J. Phys. Chem. A 107 (2003) 10303–10310.
[11] R. Liyanage, M.L. Styles, R.A.J. O'Hair, P.B. Armentrout, Sequential bond energies of $Pt^+(NH_3)_x$ (x=1-4) determined by collision-induced dissociation and theory, Int. J. Mass Spectrom. 227 (2003) 47–62.
[12] M.-E. Moret, P. Chen, Ligand binding energies in cationic platinum(II) complexes: A quantitative study in the gas phase, Organometallics 26 (2007) 1523–1530.
[13] L.A. Hammad, G. Gerdes, P. Chen, Electrospray ionization tandem mass spectrometric determination of ligand binding energies in Platinum(II) complexes, Organometallics 24 (2005) 1907–1913.
[14] B. Lippert, Cisplatin: Chemistry and Biochemistry of a Leading Anticancer Drug, Wiley-VCH, Zurich, 1999.
[15] A.V. Klein, T.W. Hambley, Cisplatin in cancer therapy: molecular mechanisms of action, Chem. Rev. 109 (2009) 4911–4920.
[16] J.J. Wilson, S.J. Lippard, Synthetic methods for the preparation of platinum anticancer complexes, Chem. Rev. 114 (2014) 4470–4495.
[17] T.C. Johnstone, K. Suntharalingam, S.J. Lippard, The next generation of platinum drugs: targeted Pt(II) agents,nanoparticle delivery, and Pt(IV) prodrugs, Chem. Rev. 116 (2016) 3436–3486.
[18] Z.D. Bugarcic, J. Bogojeski, B. Petrovic, S. Hochreuther, R. van Eldik, Mechanistic studies on the reactions of platinum(II) complexes with nitrogen- and sulfur-donor biomolecules, Dalton Trans. 41 (2012) 12329–12345.
[19] D.V. Deubel, Factors governing the kinetic competition of nitrogen and sulfur ligands in cisplatin binding to biological targets, J. Am. Chem. Soc. 126 (2004) 5999–6004.
[20] A. Casini, J. Reedijk, Interactions of anticancer Pt compounds with proteins: an overlooked topic in medicinal inorganic chemistry? Chem. Sci. 3 (2012) 3135–3144.
[21] Y. Du, N. Zhang, M. Cui, Z. Liu, S. Liu, Investigation on the hydrolysis of the anticancer drug cisplatin by Fourier transform ion cyclotron resonance mass spectrometry, Rapid Commun. Mass Spectrom. 26 (2012) 2832–2836.
[22] M. Cui, L. Ding, Z. Mester, Separation of cisplatin and its hydrolysis products using electrospray ionization high-field asymmetric waveform ion mobility spectrometry coupled with ion trap mass spectrometry, Anal. Chem. 75 (2003) 5847–5853.
[23] A. De Petris, A. Ciavardini, C. Coletti, N. Re, B. Chiavarino, M.E. Crestoni, S. Fornarini, Vibrational signatures of the naked aqua complexes from Platinum(II) anticancer drugs, J. Phys. Chem. Lett. 4 (2013) 3631–3635.
[24] D. Corinti, C. Coletti, N. Re, S. Piccirillo, M. Giampà, M.E. Crestoni, S. Fornarini, Hydrolysis of cis- and transplatin: structure and reactivity of the aqua complexes in a solvent free environment, RSC Adv. 7 (2017) 15877–15884.
[25] B. Chiavarino, M.E. Crestoni, S. Fornarini, D. Scuderi, J.-Y. Salpin, Interaction of cisplatin with adenine and guanine: a combined IRMPD, MS/MS and theoretical study, J. Am. Chem. Soc. 135 (2013) 1445–1455.
[26] B. Chiavarino, M.E. Crestoni, S. Fornarini, D. Scuderi, J.-Y. Salpin, Interaction of cisplatin with dGMP : a combined IRMPD and theoretical study, Inorg. Chem. 54 (2015) 3513–3522.
[27] B. Chiavarino, M.E. Crestoni, S. Fornarini, D. Scuderi, J.-Y. Salpin, Undervalued N3-coordination revealed in the cisplatin complex with 2′-deoxyadenosine-5′-monophosphate by a combined IRMPD and theoretical study, Inorg. Chem. 56 (2017) 8793–8801.
[28] R. Paciotti, D. Corinti, A. De Petris, A. Ciavardini, S. Piccirillo, C. Coletti, N. Re, P. Maitre, B. Bellina, P. Barran, B. Chiavarino, M.E. Crestoni, S. Fornarini, Cisplatin and transplatin interaction with methionine: bonding motifs assayed by vibrational spectroscopy in the isolated ionic complexes, Phys. Chem. Chem. Phys. 19 (2017) 26697–26707.
[29] D. Corinti, A. De Petris, C. Coletti, N. Re, B. Chiavarino, M.E. Crestoni, S. Fornarini, Cisplatin primary complex with L-histidine target revealed by IRMPD spectroscopy, ChemPhysChem 18 (2017) 318–325.
[30] D. Corinti, C. Coletti, N. Re, B. Chiavarino, M.E. Crestoni, S. Fornarini, Cisplatin binding to biological ligands revealed at the encounter complex level by IR action spectroscopy, Chem. Eur. J. 22 (2016) 3794–3803.
[31] D.T. Richens, Ligand substitution reactions at inorganic centers, Chem. Rev. 105 (2005) 1961–2002.
[32] S. Dong, W. Shi, J. Zhang, S. Bi, Theoretical studies of the formation mechanisms, thermodynamic stabilities, and water-exchange reactivities of aluminum-salicylate complexes in aqueous solution, ACS Earth Space Chem. 2 (2018) 422–431.
[33] A.S. Ten, N. Humbert, B. Verdejo, J.M. Llinares, M. Elhabiri, J. Jerzierska, C. Soriano, H. Kozlovski, A.-M. Albrecht-Gary, E. García-España, Cu^{2+}coordination properties of a 2-pyridine heptaamine tripod: Characterization and binding mechanism, Inorg. Chem. 48 (2009) 8985–8997.
[34] C. Bremer, H. Ruf, E. Grell, Kinetics and mechanism of complex formation between $Mg^{2+}$and methylthymol blue, J. Phys. Chem. A 102 (1998) 146–152.
[35] Z. Szabó, J. Glaser, I. Grenthe, Kinetics of ligand exchange reactions for uranyl(2+) fluoride complexes in aqueous solution, Inorg. Chem. 35 (1996) 2036–2044.
[36] S.J. Berners-Price, T.G. Appleton, The chemistry of cisplatin in aqueous solution, in: L.R. Kelland, N.P. Farrell (Eds.), Platinum-Based Drugs in Cancer Therapy. Cancer Drug Discovery and Development, Humana Press, Totowa, NJ, 2000, pp. 3–35.
[37] J.M. Bakker, T. Besson, J. Lemaire, D. Scuderi, P. Maître, Gas-phase structure of a -allyl-palladium complex: efficient infrared spectroscopy in a 7 T Fourier transform mass spectrometer, J. Phys. Chem. A 111 (2007) 13415–13424.
[38] C. Coletti, N. Re, D. Scuderi, P. Maitre, B. Chiavarino, S. Fornarini, F. Lanucara, R.K. Sinha, M.E. Crestoni, IRMPD spectroscopy of protonated S-nitrosocaptopril, a biologically active, synthetic amino acid, Phys. Chem. Chem. Phys. 12 (2010) 13455–13467.
[39] A. Filippi, C. Fraschetti, S. Piccirillo, F. Rondino, B. Botta, I. D'Acquarica, A. Calcaterra, M. Speranza, Chirality effects on the IRMPD spectra of basket resorcinarene/nucleoside complexes, Chem. Eur. J. 18 (2012) 8320–8328.
[40] J. Lemaire, P. Boissel, M. Heninger, G. Mauclaire, G. Bellec, H. Mestdagh, A. Simon, S. Le Caer, J.M. Ortega, F. Glotin, P. Maitre, Gas phase infrared spectroscopy of selectively prepared ions, Phys. Rev. Lett. 89 (2002), 273002.
[41] C.C. He, B. Kimutai, X. Bao, L. Hamlow, Y. Zhu, S.F. Strobehn, J. Gao, G. Berden, J. Oomens, C.S. Chow, M.T. Rodgers, Evaluation of hybrid theoretical approaches for structural determination of a glycine-linked cisplatin

derivative via infrared multiple photon dissociation (IRMPD) action spectroscopy, J. Phys. Chem. A 119 (2015) 10980–10987.
[42] P.J. Hay, W.R. Wadt, Ab initio effective core potentials for molecular calculations. Potentials for K to Au including the outermost core orbitals, J. Chem. Phys. 82 (1985) 299–310.
[43] H. Schwarz, Relativistic effects in gas-phase ion chemistry: an experimentalist's view, Angew. Chem. Int. Ed. 42 (2003) 4442–4454.
[44] M.J. Frisch, G.W. Trucks, H.B. Schlegel, G.E. Scuseria, M.A. Robb, J.R. Cheeseman, G. Scalmani, V. Barone, B. Mennucci, G.A. Petersson, H. Nakatsuji, M. Caricato, X. Li, H.P. Hratchian, A.F. Izmaylov, J. Bloino, G. Zheng, J.L. Sonnenberg, M. Hada, M. Ehara, K. Toyota, R. Fukuda, J. Hasegawa, M. Ishida, T. Nakajima, Y. Honda, O. Kitao, H. Nakai, T. Vreven, J.A. Montgomery Jr., J.E. Peralta, F. Ogliaro, M. Bearpark, J.J. Heyd, E. Brothers, K.N. Kudin, V.N. Staroverov, R. Kobayashi, J. Normand, K. Raghavachari, A. Rendell, J.C. Burant, S.S. Iyengar, J. Tomasi, M. Cossi, N. Rega, J.M. Millam, M. Klene, J.E. Knox, J.B. Cross, V. Bakken, C. Adamo, J. Jaramillo, R. Gomperts, R.E. Stratmann, O. Yazyev, A.J. Austin, R. Cammi, C. Pomelli, J.W. Ochterski, R.L. Martin, K. Morokuma, V.G. Zakrzewski, G.A. Voth, P. Salvador, J.J. Dannenberg, S. Dapprich, A.D. Daniels, Ö. Farkas, J.B. Foresman, J.V. Ortiz, J. Cioslowski, D.J. Fox, Gaussian09, Revision D.01, Gaussian, Inc., Wallingford CT, 2009.
[45] A. Casini, G. Mastrobuoni, C. Temperini, C. Gabbiani, S. Francese, G. Moneti, C.T. Supuran, A. Scozzafava, L. Messori, ESI mass spectrometry and X-ray diffraction studies of adducts between anticancer platinum drugs and hen egg white lysozyme, Chem. Commun. 14 (2007) 156–158.
[46] H. Li, Y. Huilin, H.I.A. Zhao, Y. Phillips, T.-Y. Qi, P.J. Lin, P.B. Sadler, O'Connor, Mass spectrometry evidence for cisplatin as a protein cross-linking reagent, Anal. Chem. 83 (2011) 5369–5376.
[47] Z. Xu, J.S. Brodbelt, Differentiation and distributions of DNA/cisplatin crosslinks by liquid chromatography-electrospray ionization-infrared multiphoton dissociation mass spectrometry, J. Am. Soc. Mass Spectrom. 25 (2014) 71–79.
[48] C.G. Hartinger, Y.O. Tsybin, J. Fuchser, P.J. Dyson, Characterization of platinum anticancer drug protein-binding sites using a top-down mass spectrometric approach, Inorg. Chem. 47 (2008) 17–19.
[49] L. Feketeova, V. Ryzhov, R.A.J. O'Hair, Comparison of collision- versus electron-induced dissociation of Pt(II) ternary complexes of histidine- and methionine-containing peptides, Rapid Commun. Mass Spectrom. 23 (2009) 3133–3143.
[50] L. Jašíková, J. Roithová, Infrared multiphoton dissociation spectroscopy with free-electron lasers: on the road from small molecules to biomolecules, Chem. Eur. J. 24 (2018) 3374–3390.
[51] A. Zehnacker, Optical spectroscopy coupled with mass spectrometry methods, Phys. Chem. Chem. Phys. 17 (2015) 25672–25675.
[52] Laser photodissociation and spectroscopy of mass-separated biomolecular ions, in: N.C. Polfer, P. Dugourd (Eds.), Lecture Notes in Chemistry, vol. 83, Springer, 2013.
[53] N.C. Polfer, J. Oomens, Vibrational spectroscopy of bare and solvated ionic complexes of biological relevance, Mass Spectrom. Rev. 28 (2009) 468–494.
[54] J.R. Eyler, Infrared multiple photon dissociation spectroscopy of ions in penning traps, Mass Spectrom. Rev. 28 (2009) 448–467.
[55] L. MacAleese, P. Maitre, Infrared spectroscopy of organometallic ions in the gas phase: from model to real world complexes, Mass Spectrom. Rev. 26 (2007) 583–605.
[56] J. Oomens, B.G. Sartakov, G. Meijer, G. von Helden, Gas-phase infrared multiple photon dissociation spectroscopy of mass-selected molecular ions, Int. J. Mass Spectrom. 254 (2006) 1–19.
[57] Z.D. Bugarcic, J. Bogojeski, B. Petrovic, S. Hochreuther, R. van Eldik, Mechanistic studies on the reactions of platinum(II) complexes with nitrogen and sulfur-donor biomolecules, Dalton Trans. 41 (2012) 12329–12345.
[58] A. Zehnacker, Chirality effects in gas-phase spectroscopy and photophysics of molecular and ionic complexes: contribution of low and room temperature studies, Int. Rev. Phys. Chem. 33 (2014) 151–207.
[59] L. Voronina, T.R. Rizzo, Spectroscopic studies of kinetically trapped conformations in the gas phase: the case of triply protonated bradykinin, Phys. Chem. Chem. Phys. 17 (2015) 25828–25836.
[60] R.J. Cross, Ligand substitution reactions of square-planar molecules, Chem. Soc. Rev. 14 (1985) 197–223.
[61] S.F. Lincoln, A.E. Merbach, Substitution reactions of solvated metal ions, Adv. Inorg. Chem. 42 (1995) 1–88.
[62] J. Bergès, I. Fourré, J. Pilmé, J. Kozelka, Quantum chemical topology study of the water-platinum(II) interaction, Inorg. Chem. 52 (2013) 1217–1227.
[63] J. Fedoce Lopes, W.R. Rocha, H.F. Dos Santos, W.B. De Almeida, Theoretical study of the potential energy surface for the interaction of cisplatin and their aquated species with water, J. Chem. Phys. 128 (2008), 165103.
[64] L.A. Sodré Costa, W.R. Rocha, W.B. De Almeida, H.F. Dos Santos, The hydrolysis process of the cis-dichloro(ethylenediamine)platinum(II): a theoretical study, J. Chem. Phys. 118 (2003) 10584.
[65] D.V. Deubel, Factors governing the kinetic competition of nitrogen and sulfur ligands in cisplatin binding to biological targets, J. Am. Chem. Soc. 126 (2004) 5999–6004.
[66] Z. Chval, M. Sip, Pentacoordinated transition states of cisplatin hydrolysis - ab initio study, J. Mol. Struct. (Theochem) 532 (2000) 59–68.
[67] S. Banerjee, P. Sarathi Sengupta, A.K. Mukherjee, A detailed theoretical study of the interaction of thiourea with cis-diaqua(ethylenediamine) platinum(II), J. Mol. Struct. (Theochem) 913 (2009) 97–106.
[68] A. de Cjzar, O. LarraÇaga, F.M. Bickelhaupt, E. San Sebastian, E. Ortega-Carrasco, J.-D. Marechal, A. Lledos, F.P. Cossio, New insights into the reactivity of cisplatin with free and restrained nucleophiles: microsolvation effects and base selectivity in cisplatin–DNA interactions, ChemPhysChem 17 (2016) 3932–3947.
[69] Z. Chval, M. Sip, J.V. Burda, The trans effect in square-planar platinum(II) complexes-a density functional study, J. Comput. Chem. 29 (2008) 2370–2381.
[70] For example, see: D. M. Roddick, D. Zargarian, Pentacoordination for pincer and related terdentate coordination compounds: Revisiting structural properties and trends for d8 transition metal systems, Inorg. Chim. Acta 422 (2014) 251–264.